

Hierarchical Graphical Models for Multigroup Shape Analysis using Expectation Maximization with Sampling in Kendall's Shape Space

Yen-Yun Yu, P. Thomas Fletcher and Suyash P. Awate

Scientific Computing and Imaging (SCI) Institute

University of Utah.

Dec. 15. 2012

Abstract

This paper proposes a novel framework for multigroup shape analysis relying on a *hierarchical* graphical statistical model on shapes within a population. The framework represents individual *shapes* as pointsets modulo translation, rotation, and scale, following the notion in Kendall's shape space. While individual shapes are derived from their group shape model, each group shape model is derived from a single population shape model. The hierarchical model follows the natural organization of population data and the top level in the hierarchy provides a common frame of reference for multigroup shape analysis, e.g. classification and hypothesis testing. Unlike typical shape-modeling approaches, the proposed model is a *generative* model that defines a joint distribution of object-boundary data and the shape-model variables. Furthermore, it naturally enforces optimal correspondences during the process of model fitting and thereby subsumes the so-called *correspondence problem*. The proposed inference scheme employs an expectation maximization (EM) algorithm that treats the individual and group shape variables as hidden random variables and integrates them out before estimating the parameters (population mean and variance and the group variances). The underpinning of the EM algorithm is the *sampling of pointsets, in Kendall's shape space*, from their posterior distribution, for which we exploit a highly-efficient scheme based on Hamiltonian Monte Carlo simulation. Experiments in this paper use the fitted hierarchical model to perform (1) *hypothesis testing* for comparison between pairs of groups using permutation testing and (2) *classification* for image retrieval. The paper validates the proposed framework on simulated data and demonstrates results on real data.

Introduction and Related Work

Shape modeling and analysis is an important problem in a variety of fields including biology, medical image analysis, and computer vision[1, 7, 9, 12] that has received considerable attention over the last few decades. Kendall[12] defines *shape* as an equivalence class of pointsets under the similarities generated by translation, rotation, and scaling. Objects in biological images or anatomical structures in medical images often possess shape as the sole identifying characteristic instead of color or texture. Applications of shape analysis beyond natural contexts include handwriting analysis and character recognition. In the medical context, shapes of human anatomical structures can provide crucial cues in diagnosis of pathologies or disorders. The key problems in this context lie in the fitting of shape models to population image data followed by statistical analysis such as hypothesis testing to compare groups, classification of unseen shapes in one of the groups for which the shape models are learnt, or unsupervised clustering of shapes.

A variety of applications of shape analysis deal with population data that naturally calls for a *hierarchical* modeling approach. First, the hierarchical model follows the natural organization or structure of the data. For instance, as in Figure 1, the model variables at the top level capture statistical properties of the population (e.g., individuals with and without medical conditions), the model variables at a lower level capture statistical properties of different groups within a population (e.g., clinical cohorts based on gender or age or type of disease within a spectrum disorder), and the model variables at the lowest level capture individual properties, which finally relate to the observed data. Second, the top-level population variables are necessary to enable comparison (through hypothesis testing or classification) between the groups within the population because the population shape variable helps provide a common reference frame (e.g., a grand mean) for the shape models underlying different groups.

Previous works on "hierarchical" (overloaded term) shape modeling concern (i) multi-resolution/scale models e.g., face model at fine-to-coarse resolutions) or (ii) multi-part models (e.g., car decomposed into body, tires, hood, trunk) with inter-part spatial relationships. In contrast, our proposed model is the first hierarchical probabilistic model comprising a population with multiple groups (e.g., vehicle population comprising sedans, trucks, buses).

In the context of image-based applications, shape models are constructed from image-derived data that is typically in the form of a set of pixels lying close to the object boundary detected in the set of images; each pointset has the same number of points (also interpreted as *landmarks*[7]). To obtain valid and useful shape models from the data, it is crucial to determine (i) the positions of the points, within each pointset, in relationship to the object boundary in the image, and (ii) meaningful *correspondences*[7] of points across pointsets in the group and the population. Some of the early approaches to shape modeling[3, 9] assumed knowledge

arXiv:1212.5720v2 [cs.CV] 10 Jan 2013

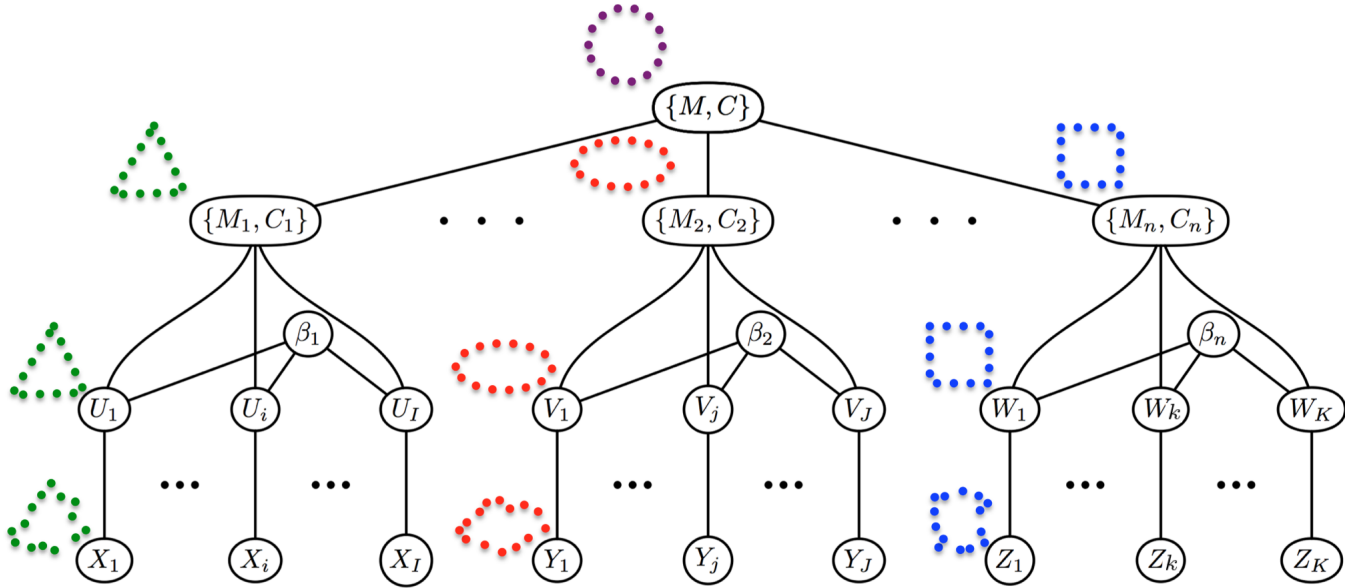


Figure 1: **Hierarchical Modeling of Multiple Groups of Shapes in a Population.**

of a set of homologous landmarks, typically manually defined, comprising the pointset for each object in the population. They proposed methods for learning Gaussian shape models for such landmark data observed for a population. However, for shapes that are complex or 3 dimensional, manually defining landmarks can be infeasible and inaccurate. Thus, there is a need to include the pointsets, describing each individual shape in the population, as variables in an optimization process. Several approaches to the correspondence problem attempt to find the *simplest* explanation for the point positions, including methods based on the logarithm of the determinant of the model covariance matrix[13], minimum description length[5, 21], and minimum entropy[2, 19]. While these model-building criteria are based on statistical properties of the pointsets, (i) none of these approaches use *generative* statistical models, (ii) they force correspondences in an adhoc manner by introducing adhoc terms in the objective function, and (iii) have 2 independent stages where the first finds optimal correspondences and the second estimates model parameters.

Some generative model approaches to shape have been introduced in the computer vision literature[4, 10, 20, 18, 23], but these are defined relative to some pre-determined template shape with manually-placed landmarks. On the other hand, the proposed method learns shape models from populations of detected object boundaries in images, without any a priori definition of a template or known landmarks. Furthermore, it proposes a generative statistical model for hierarchical shape modeling that naturally enforces optimal correspondences as a result of model fitting. In this way, the proposed modeling and optimization framework subsumes the correspondence problem.

This paper makes several contributions. First, it proposes a novel hierarchical generative statistical model for modeling shapes within a population. This model tightly couples each individual shape model to the observed data (i.e., the set of points on the object boundary detected in the image) by designing their joint distribution using the (nonlinear) *current norm* between pointsets[11, 22]. Second, the proposed optimization framework employs an *expectation maximization* (EM) algorithm[6] that treats the individual and group shape variables as hidden random variables and integrates them out before estimating the parameters, which are population mean and variance and the group variances. In this way, the proposed Bayesian EM-based inference framework is an improvement over using the mode approximation for the hidden variables. Third, the underpinning of the EM algorithm is the sampling of shapes (within Kendall shape space) from their posterior PDFs, e.g., shape variables for individual data have posterior PDFs involving (i) likelihood PDFs designed using the (nonlinear) current norm and (ii) prior PDFs conditioned on the group shape mean. For this purpose, this paper exploits a novel highly-efficient sampling scheme relying on *Hamiltonian Monte Carlo* (HMC) simulation[8, 15][16][17].

The remainder of the paper is organized as follows. Section 2 gives an overview of the proposed hierarchical statistical generative model for multigroup population data. Section 3 presents the EM formulation for the optimization problem. It defines the hidden variables and the parameters and the joint PDF, the details of the expectation step for integrating over the hidden variables, involving the HMC approach, and the subsequent maximization step to optimize the parameters. Section 6 describes a hypothesis-testing scheme, using permutation testing, for comparing any pairs of groups within the population. Section 7 presents a method for shape classification. Section 8 summarizes the paper.

2 Hierarchical Multigroup Shape Model

This section gives an overview of the proposed hierarchical statistical generative model for multigroup population data, illustrated in Figure 1.

Let the group of random variables $X \triangleq \{X_i\}_{i=1,\dots,I}$ model *observed data* where each (vector) random variable X_i is a set of observed (corrupted) points (representing shape) on the boundary of the i^{th} structure. That is, $X_i \triangleq \{X_i(t)\}_{t=1,\dots,T}$ where $X_i(t) \in \mathbb{R}^D$ is the D -dimensional coordinate of the t^{th} point on the boundary of the i^{th} structure. We assume that all I random variables X_i belong to a *single group* of shapes, with the group's shape model given by variables $\{M_1, C_1\}$ where M_1 is the mean shape and C_1 the covariance of the shapes in the group.

Similarly, we have other groups of shapes modeled by analogous random variables, e.g., group $Y \triangleq \{Y_j\}_{j=1,\dots,J}$ with group mean and covariance $\{M_2, C_2\}$, group $\{Z_k\}_{k=1,\dots,K}$ with group mean and covariance $\{M_3, C_3\}$, etc. In order to be able to perform shape classification or hypothesis testing between groups, we ensure that the shape models lie in the same space by enforcing the same number of points T in all group shape means, i.e., $M_1 \triangleq \{M_1(t)\}_{t=1,\dots,T}$, $M_2 \triangleq \{M_2(t)\}_{t=1,\dots,T}$, etc. all have the same number of points T . Thus, $M_1 \in \mathbb{R}^{TD}$, $M_2 \in \mathbb{R}^{TD}$, $M_3 \in \mathbb{R}^{TD}$, $\forall i X_i \in \mathbb{R}^{TD}$, $\forall j Y_j \in \mathbb{R}^{TD}$, and $\forall k Z_k \in \mathbb{R}^{TD}$. Furthermore, we assume that all groups belong to a single population of shapes with shape parameters $\{M, C\}$ that represent the mean and covariance on the group means M_1, M_2 , etc.

In the rest of the formulation, without loss of generality, we consider two groups for simplicity. For each group of shapes, we need to model the joint PDF comprising the population model variables M, C , group-level model variables M_1, C_1, M_2, C_2 , and the data X, Y , i.e., $P(M, C, M_1, C_1, M_2, C_2, X, Y)$. Given observed data x, y that comprises sets of shapes within 2 groups, the problem addressed in this paper is to fit the aforementioned hierarchical multigroup shape model to the data and subsequently perform hypothesis testing or classification.

3 Inference via Monte-Carlo Expectation Maximization

We solve the multigroup shape-fitting problem using the EM framework[6]. Figure 1 gives an overview of the approach.

For the first group, i.e., corresponding to X , we assume a *hidden* random variable $U \triangleq \{U_i\}_{i=1,\dots,I}$ where each (vector) random variable U_i represents the Kendall shape corresponding to the observed data x_i . The number of points in U_i is the same as those in M_1 , i.e., T points. Similarly, we assume a hidden variable V for the second group. We also consider the group means M_1, M_2 as hidden (Kendall-shape) variables. The *parameters* in our model include the group-specific covariances C_1, C_2 , the population mean M and the population covariance C . We introduce parameters β_1, β_2 , one per group, to control the smoothness of the hidden shape variables U_i, V_j . In this paper, (i) β_1, β_2 are fixed to 1 and (ii) smoothness parameters are ignored for the group means because of their limited practical utility. Let $\theta \triangleq \{C_1, C_2, M, C\}$ be the set of parameters to be estimated. Then, the inference problem is:

$$\begin{aligned} \max_{\theta} P(x, y|\theta) = \\ \max_{\theta} \int P(U, V, M_1, M_2, x, y|\theta) du dv dm_1 dm_2 \end{aligned} \quad (1)$$

In the i^{th} iteration of EM optimization, with the parameter estimate $\hat{\theta}^i$, the E step constructs the *Q function*

$$\begin{aligned} Q(\theta|\hat{\theta}^i) \triangleq \\ E_{P(U, V, M_1, M_2|x, y, \hat{\theta}^i)} \log P(U, V, M_1, M_2, x, y|\theta). \end{aligned} \quad (2)$$

which, because of the intractability of the expectation, we approximate using Monte-Carlo simulation as follows:

$$\begin{aligned} Q(\theta|\hat{\theta}^i) \approx \hat{Q}(\theta|\hat{\theta}^i) \triangleq \sum_{s=1}^S \frac{1}{S} \log P(u^s, v^s, m_1^s, m_2^s, x, y|\theta), \\ \text{where } (u^s, v^s, m_1^s, m_2^s) \sim P(U, V, M_1, M_2|x, y, \hat{\theta}^i) \end{aligned} \quad (3)$$

and where shapes u, v , which correspond to each observed sets of boundary points X, Y , as well as shapes m_1, m_2 , which correspond to the group means, are sampled from the posterior $P(U, V, M_1, M_2|x, y, \hat{\theta}^i)$.

In the EM framework, with the hidden variables U, V , we model the joint PDF comprising the population shape variables, per-group shape variables, per-individual shape variables, and the data as:

$$\begin{aligned} P(M, C, M_1, C_1, M_2, C_2, U, V, X, Y) \triangleq \\ P(M, C, C_1, C_2) P(M_1|M, C) P(M_2|M, C) \\ \prod_{i=1}^I P(U_i|M_1, C_1, \beta_1) P(X_i|U_i) \\ \prod_{j=1}^J P(V_j|M_2, C_2, \beta_2) P(Y_j|V_j), \text{ where} \end{aligned} \quad (4)$$

- $P(M, C, C_1, C_2)$ is a prior on the population shape mean and covariance and the per-group shape covariances (ignored in this paper).
- $P(M_1|M, C), P(M_2|M, C)$ are modelled as Gaussians with mean M and covariance C .
- We design $P(U_i|M_1, C_1, \beta_1)$ (and similarly $P(V_j|M_2, C_2, \beta_2)$) so as to penalize (i) the Mahalanobis distance of U_i under M_1, C_1 as well as the (ii) deviation of every individual point $U_i(t)$ given its neighbors. For structures in 2-dimensional images ($D = 2$ in this paper) whose boundaries are planar closed curves, the neighborhood system underlying shape variable U_i (which comprises points $\{U_i(t)\}$) assigns two neighbors to each point: i.e., neighbors of $t : \forall 2 \leq t \leq (T - 1)$ are $(t - 1)$ and $(t + 1)$, neighbors of $t = 1$ are $t = T$ and $t = 2$, and neighbors of $t = T$ are $t = (T - 1)$ and $t = 1$. Given this neighborhood system $\mathcal{N} \triangleq \{(t_1, t_2) : t_1, t_2 \text{ are neighbors}\}$,

$$\begin{aligned}
& P(U_i|M_1, C_1, \beta_1) \triangleq \\
& \frac{1}{Z} \exp \left(-0.5(U_i - M_1)'C_1^{-1}(U_i - M_1) \right. \\
& \quad \left. - \beta_1 \sum_{(t_1, t_2) \in \mathcal{N}} \|U_i(t_1) - U_i(t_2)\|^2 \right) \tag{5}
\end{aligned}$$

where β_1 controls the level of smoothness ($\beta_1 = \beta_2 = 1$ in this paper) and Z is the partition function.

- $P(X_i|U_i), P(Y_j|V_j)$ are modelled using the current norm as follows. Consider two pointsets $A = \{a_i\}_{i=1, \dots, I}$ and $B = \{b_j\}_{j=1, \dots, J}$. Given a kernel similarity function $K(\cdot)$, which is Gaussian in this paper, the squared current norm between A and B is:

$$\begin{aligned}
d_k^2(A, B) \triangleq & \sum_{i'=1}^I \sum_{i''=1}^I K(a_{i'}, a_{i''}) + \\
& \sum_{j'=1}^J \sum_{j''=1}^J K(b_{j'}, b_{j''}) - 2 \sum_{i=1}^I \sum_{j=1}^J K(a_i, b_j). \tag{6}
\end{aligned}$$

We exploit the current norm to define a PDF on data shapes X_i given shape variables U_i as follows:

$$P(X_i|U_i) \triangleq \frac{1}{\gamma} \exp \left(-d_k^2(X_i, U_i) \right), \tag{7}$$

where γ is a suitable normalization factor. Note: this allows the number of points in the shape models to be different from the number of observed boundary points.

3.1 E Step: Sampling in Shape Space using Hamiltonian Monte Carlo

In EM optimization, the E step requires sampling the hidden variables U, V, M_1, M_2 from the posterior PDF $P(U, V, M_1, M_2|x, y, \hat{\theta}^i)$. We employ the Hamiltonian Monte Carlo procedure[8][16][17] for this sampling. HMC is a highly efficient sampling technique that belongs to the class of Markov-chain Monte-Carlo samplers. HMC exploits the gradient of the energy function (i.e., $\log P(U, V, M_1, M_2|x, y, \hat{\theta}^i)$, in our case) for fast exploration of the space of the hidden random variables. The key idea underlying HMC is to first augment the original variables with auxiliary momentum variables, then define a Hamiltonian function combining the original and auxiliary variables, and, subsequently, alternate between simple updates for these auxiliary momentum variables and Metropolis updates for the original variables. HMC proposes new states by computing a trajectory according Hamiltonian dynamics implemented with a leapfrog method. Such new states can be very distant from the current states, thereby leading to a fast exploration of the state space. Furthermore, Hamiltonian dynamics theoretically guarantees that the new proposal states are accepted with high probability. We sample the set of hidden variables U, V, M_1, M_2 by successively sampling the variables $\{U_i\}, \{V_j\}, \{M_1\}, \{M_2\}$, following a Gibbs sampling technique, where each variable is sampled using HMC. The HMC procedure requires gradients of the energy function $\log P(U, V, M_1, M_2|x, y, \hat{\theta}^i)$ with respect to the hidden variables $\{U_i\}, \{V_j\}, M_1, M_2$. The gradient of $\log P(U, V, M_1, M_2|x, y, \hat{\theta}^i)$ with respect to the group mean shape variables M_1, M_2 as well as the shape variables U_i, V_j is straightforward.

Sampling in Kendall Shape Space using HMC: In general, the gradient of the log posterior for each point t in the shape U_i can change the translation, scale, and pose/rotation for the pointset. Specifically, the smoothness penalty on the shape variables, e.g., u_i , through β_1 , tends to move the t^{th} point $u_i(t)$, to the mean of its neighbors, thereby shrinking the pointset. These effects are undesirable and significantly reduce the efficiency of the shape-sampling scheme by preventing sampling restricted to Kendall shape space. To avoid this effect, we propose to replace the gradient of the log posterior, within HMC, by a *projected gradient* that restricts the updated shape to Kendall shape space by removing effects of translation, scale, and rotation from the HMC update. Figure 2 illustrates this process. Without loss of generality, we assume that (i) u_i is centered, i.e., $\sum_t u_i(t) = \mathbf{0}$, and thus lies on a

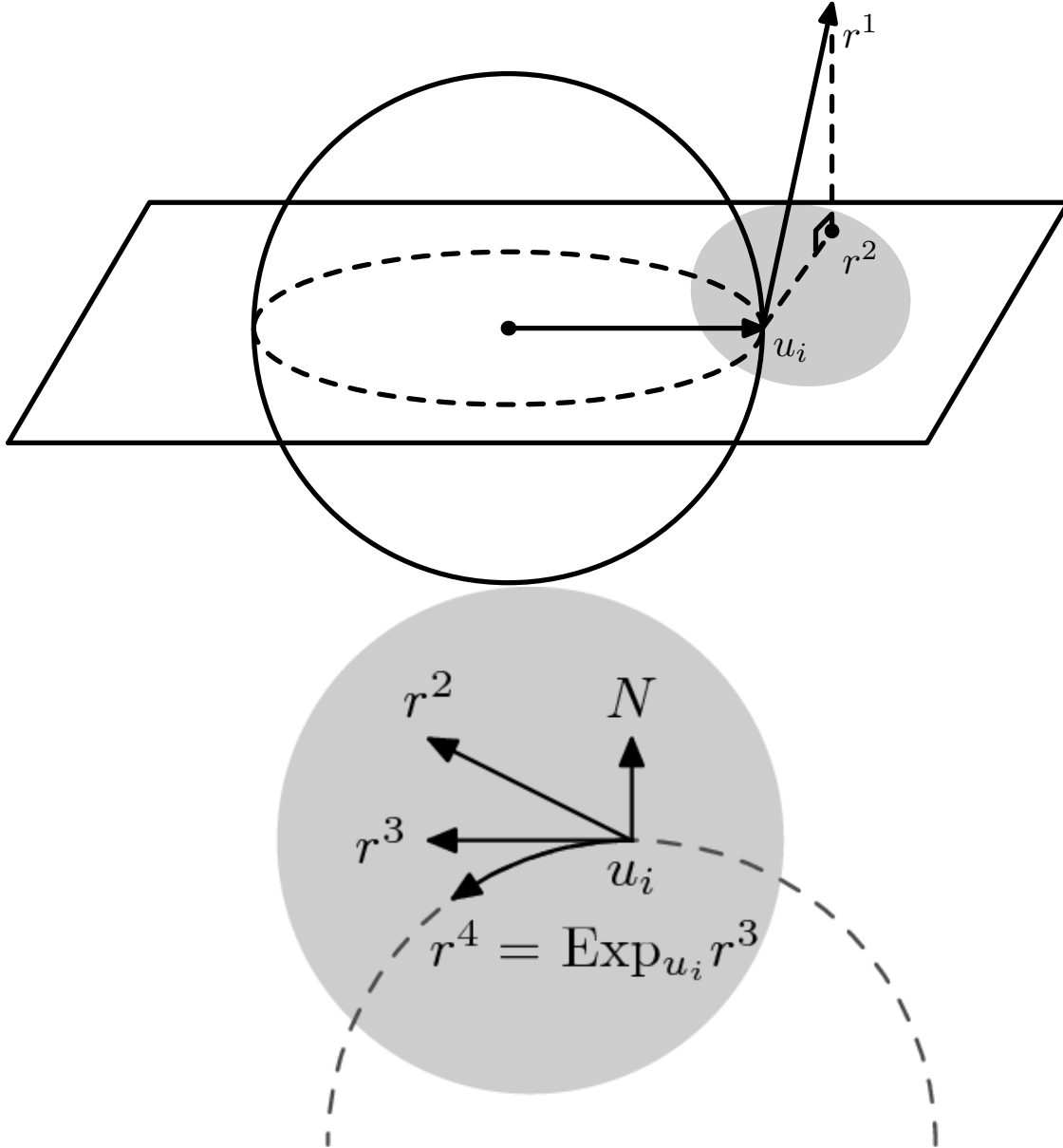


Figure 2: **Sampling in Kendall Shape Space via Gradient Projection within HMC.** **Top:** shows an illustration of Kendall’s *pre-shape* space[12] (dotted hypersphere), which is the intersection of the (bold) hypersphere of fixed radius ρ (i.e., $\sum_t \|u_i(t)\|^2 = \rho^2$; fixes scale) and the hyperplane through the origin (i.e., $\sum_t u_i(t) = 0$; fixes translation). For a pointset u_i , log-posterior gradients r^1 are projected onto the hyperplane to remove translation effects from the HMC update. **Bottom:** The resulting projection r^2 is then projected onto the tangent space at u_i , on Kendall pre-shape space (dotted hypersphere), to remove scale changes. The resulting tangent-space projection r^3 is mapped to the pre-shape space via the manifold exponential map. The resulting pre-shape r^4 is rotationally aligned with the original shape u_i , yielding r^5 (not shown in figure). These steps project the log-posterior gradient at u_i , within HMC, to generate a new sample point (not shown in figure) in Kendall shape space.

hyperplane, (ii) u_i has size ρ , i.e., $\sum_t \|u_i(t)\|^2 = \rho^2$, and thus lies on a hypersphere and (iii) u_i has a certain pose. Kendall *pre-shape* space[12] is the hypersphere (S^{TD-D} with radius ρ) that is the intersection of the hypersphere S^{TD} and the aforementioned hyperplane ($\in \mathbb{R}^{TD}$) that passes through the origin. First, we decompose the gradient for u_i into 3 components: (i) a component orthogonal to the hyperplane (this causes translation of u_i from its current location), (ii) a component within the hyperplane but orthogonal to the hypersphere (this causes changes in the size of u_i), and (iii) a component within the hyperplane and tangent to the hypersphere. Subsequently, we project the gradient vector to reduce it to the third component and then take the manifold exponential map on the hypersphere. Lastly, to remove effects of rotation, we rotationally align the resulting pointset in pre-shape space to the original pointset u_i . This gives the updated u_i in Kendall shape space.

Sampling in Hierarchical Shape Model: We generate a sample of size S as follows ($S = 100$ in this paper):

1. Set the sample index variable s to 0. Initialize the sampling procedure with the sample point $s = 0$ denoted by $u^0 \triangleq \{u_i^0\}$, $v^0 \triangleq$

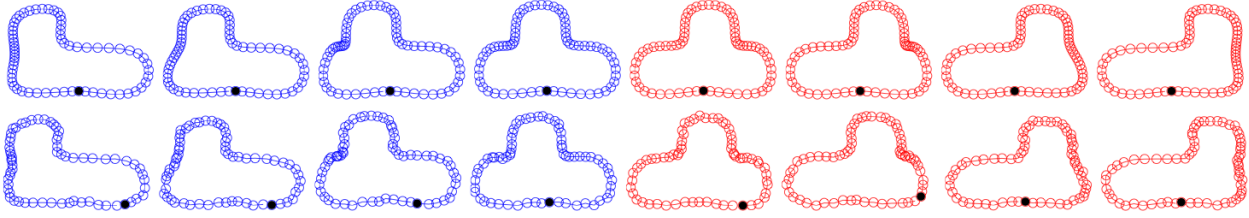


Figure 3: **Simulated Box-Bump Shapes**[13]. **Top Row:** Simulated ground-truth shape models for the 2 groups that each comprise 4 shapes. The bump for the first group (blue) is on the left while the bump for the second group (red) is on the right. Each shape has 64 points shown by circles. The black filled circle indicates the first point in the list; other points are numbered counter-clockwise. **Bottom Row:** Corrupted data where the point ordering in each shape is randomly circularly shifted (to induce poor correspondences) and independent Gaussian noise is added to each point position (to mimic errors in boundary detection).

$\{v_i^0\}, m_1^0, m_2^0$. Given sample point s , sample the $(s + 1)^{\text{th}}$ sample point as follows.

2. $\forall i$ sample $u_i^{s+1} \sim P(U_i, v^s, m_1^s, m_2^s | x, y, \hat{\theta}^i)$ via projected-gradient HMC.
3. $\forall j$ sample $v_j^{s+1} \sim P(v^s, V_j, m_1^s, m_2^s | x, y, \hat{\theta}^i)$ via projected-gradient HMC.
4. Sample $m_1^{s+1} \sim P(u^{s+1}, v^{s+1}, M_1, m_2^s | x, y, \hat{\theta}^i)$ via projected-gradient HMC.
5. Sample $m_2^{s+1} \sim P(u^{s+1}, v^{s+1}, m_1^{s+1}, M_2 | x, y, \hat{\theta}^i)$ via projected-gradient HMC.
6. If $s + 1 = S$, then stop; otherwise increment s by 1 and repeat the sampling steps.

To ensure the generation of independent samples between Gibbs iteration s and the next $s + 1$, we run the HMC procedure sufficiently long. Furthermore, as required in Gibbs sampling, we ensure independent samples between EM iteration i and the next $i + 1$ by *burning in* and discarding the first few sample points s for use in the M step.

3.2 M Step: Optimizing Parameters

In the EM optimization, at the i^{th} iteration, the M step entails maximization of the Q function $Q(\theta | \hat{\theta}^i)$ with respect to the parameters θ and sets $\hat{\theta}^{i+1} \triangleq \arg \max_{\theta} \sum_{s=1}^S \log P(u^s, v^s, m_1^s, m_2^s, x, y | \theta)$. Subsequently, we get optimal values in closed form for the parameters $\hat{C}_1^{i+1}, \hat{C}_2^{i+1}, \hat{M}^{i+1}, \hat{C}^{i+1}$:

$$\hat{C}_1^{i+1} = \frac{1}{SI} \sum_{s=1}^S \sum_{i=1}^I ((u_i^s - m_1^s)(u_i^s - m_1^s)') \quad (8)$$

$$\hat{C}_2^{i+1} = \frac{1}{SJ} \sum_{s=1}^S \sum_{j=1}^J ((v_j^s - m_2^s)(v_j^s - m_2^s)') \quad (9)$$

$$\hat{M}^{i+1} = \frac{1}{2S} \sum_{s=1}^S (m_1^s + m_2^s) \quad (10)$$

$$\hat{C}^{i+1} = \frac{1}{2S} \sum_{s=1}^S ((m_1^s - M)(m_1^s - M)' + (m_2^s - M)(m_2^s - M)') \quad (11)$$

4 Validating the Hierarchical Shape Model and Inference on Simulated Shapes

This section provides an example of a standard simulated test dataset[13] and shows that the proposed framework is able to correctly learn the true group and population models. Figure 3 (top row) shows simulated (ground-truth) pointsets, which are very similar to those used in[13], where the population is a collection of *box-bump*[13] shapes where the location of the bump (and each point) exhibits linear variation, across the group, over the top of the box. While the desired population mean M corresponds to a shape with the bump exactly in the middle, the bumps in the true group means M_1, M_2 are located symmetrically on either side of the middle. The true covariance matrices for the groups (C_1, C_2) and the population (C) have a single non-zero eigen value. Figure 3 (bottom row) shows the observed corrupted data, i.e., $\{x_i\}_{i=1}^4, \{y_j\}_{j=1}^4$, where we induce poor correspondences and noise in the point locations.

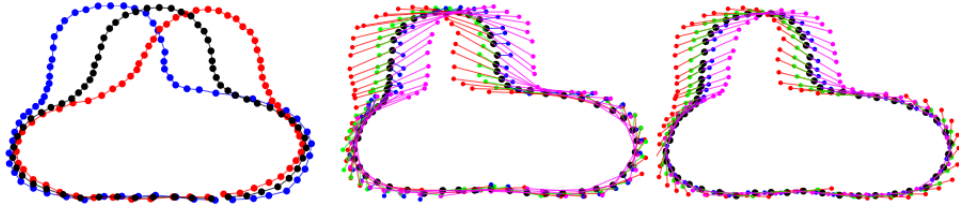


Figure 4: **Left:** shows the optimal population mean M (black dots) along with the expected values for the group means M_1 (blue dots) and M_2 (red dots) after EM inference. **Middle:** shows the **correspondence** of points for the corrupted data x_i across a selected group (blue shapes). **Right:** shows the correspondences for the expected values of shape models U_i after EM inference.

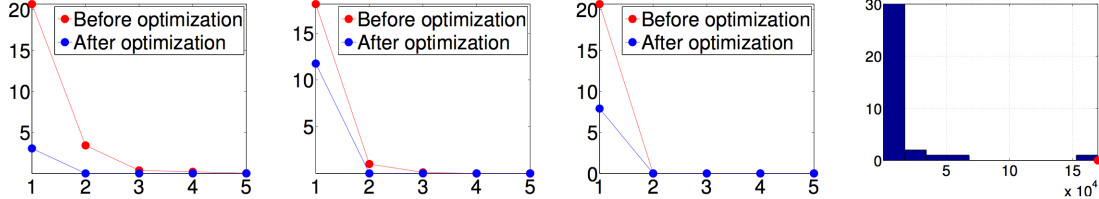


Figure 5: **3 Graphs on Left:** show the largest 5 eigen values of the covariance matrices C_1 , C , and C_2 , respectively, before and after EM optimization. **Rightmost:** shows the histogram of Hotelling's T^2 statistics obtained by permutation testing (all ${}^8C_4/2 = 35$ unique group-label permutations) and the T^2 statistic for the non-permuted groups (red dot).

Figure 4 shows the means for the groups and population after EM optimization. We see that the estimated population mean M and the expected values of the group means M_1, M_2 after EM optimization are close to their true values. Figure 4 also shows that the correspondence of corrupted data points $x_i(t)$, across the group ($i = 1, \dots, 4$), is poor, indicating a large variance. On the other hand, after EM optimization, the correspondence of the expected values of the shape variables $U_i(t)$ indicates a significantly lower variance and correctly shows the linear variation in the point location across the group.

Figure 5 shows the covariances for the groups and population after EM optimization. We see that the group covariances C_1, C_2 and the population covariance C after EM optimization indicate lower variance and a single non-zero eigen value, agreeing with the underlying true model.

5 Results of Hierarchical Shape Model and Inference on a Leaf Database

This section shows results of the proposed hierarchical multigroup shape modeling and inference on a real dataset, namely the Tree Leaf Database[14] comprising images of leaves of 90 wood species growing in the Czech Republic. We used 2 of the largest available groups comprising the species (i) *Carpinus betulus* having 23 leaf images (Figure 6; blue group) and (ii) *Fagus sylvatica* also having 23 leaf images (Figure 6; red group). The leaf stem was removed from the images manually. Interestingly, while the blue group has oblong leaves that have high curvature at one end and low at the other, the red group has oblong leaves that are more symmetric with similar curvatures at both ends.

Preprocessing: All leaf data pointsets $\{x_i\}, \{y_j\}$ initially undergo Procrustes alignment[9] to remove the effects of translation, scale, and rotation.

Figure 6 also shows the population shape mean (black) and the expected values of the group shape means (blue, red). The expected values of the shapes for the 2 groups clearly show the aforementioned subtle difference in curvatures in the leaves of the 2 species. Figure 7 shows the covariances for the leaf groups and population after EM optimization. We see that the group covariances C_1, C_2 and the population covariance C after EM optimization indicate lower variance.

6 Application I — Hypothesis Testing

After the multi-group model is fit to the data, we can perform hypothesis testing to compare any pair of groups. Since the distribution of each group is modeled by a Gaussian, e.g. $G(\cdot; M_1, C_1), G(\cdot; M_2, C_2)$, we use Hotelling's two-sample T^2 statistic to measure dissimilarity between any pair of groups. Conventionally, the p value associated with the hypothesis test is obtained by exploiting the relationship of the T^2 statistic to the F distribution with a certain degrees of freedom depending on the sample sizes (e.g. I, J , in our case) and the dimensionality (TD). In our case, however, the sample sizes ($I + J$) can be far lower than the dimensionality TD , which prevents the use of the F distribution for computing p values. Thus, we propose *permutation testing*, using the T^2 as the test statistic, for hypothesis testing to overcome the the problem of low sample size.

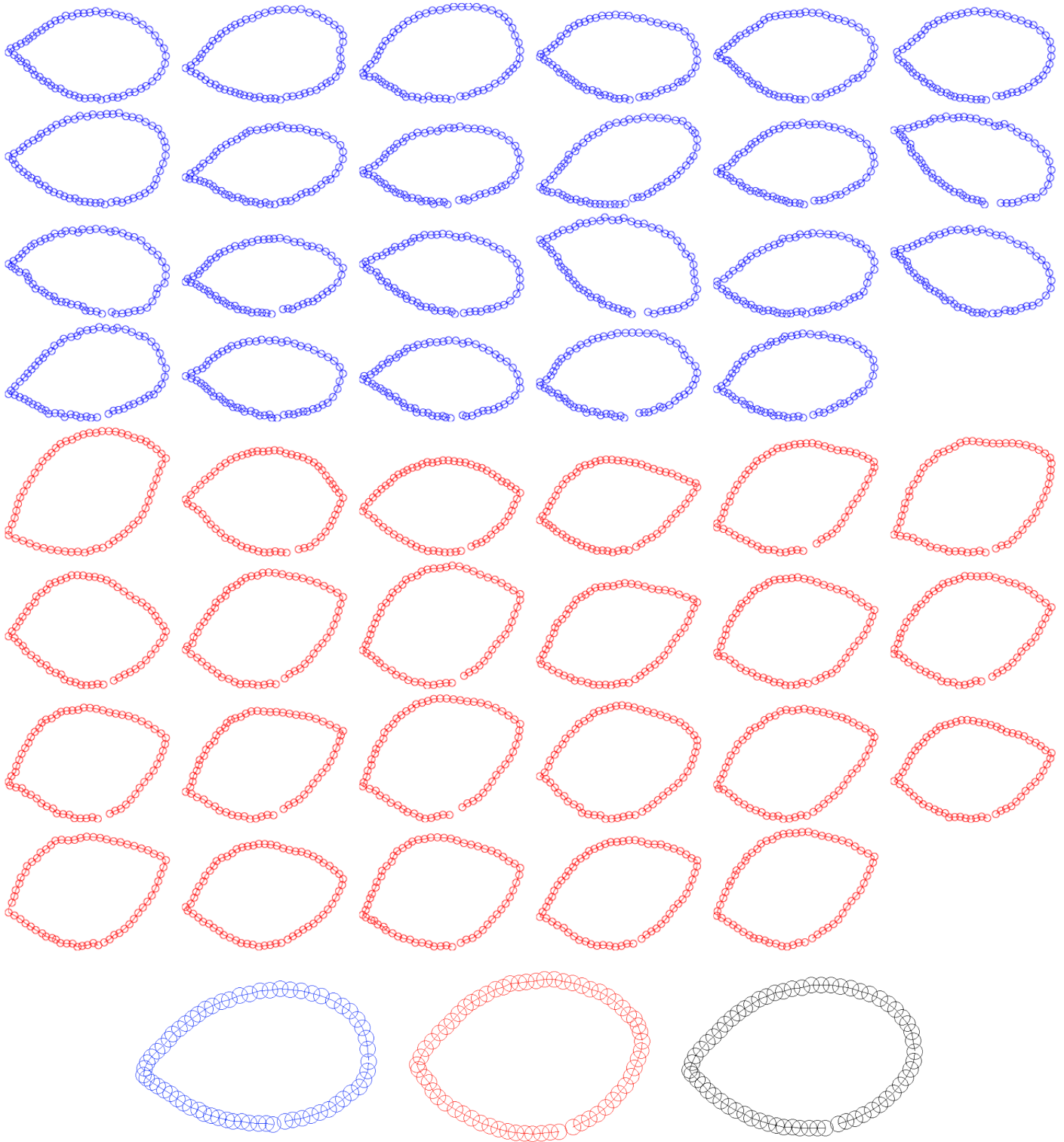


Figure 6: **Tree Leaf Database.** **Top:** shows the 2 groups of leaves from 2 different species of trees; one in red and the other in blue. **Bottom:** shows the expected values for the group-mean shape variables M_1 (blue dots) and M_2 (red dots) and the optimal population mean parameter M (black dots), after EM inference.

6.1 Validation on Simulated Data

For the simulated box-bump dataset, Figure 5 shows the expected result of permutation testing (H_0 : the 2 group models are the same) indicating the the non-permuted labeling produces the most extreme statistic (p value = $1/35 = 0.0286$) thereby leaning significantly towards rejection of the null hypothesis underlying permutation testing.

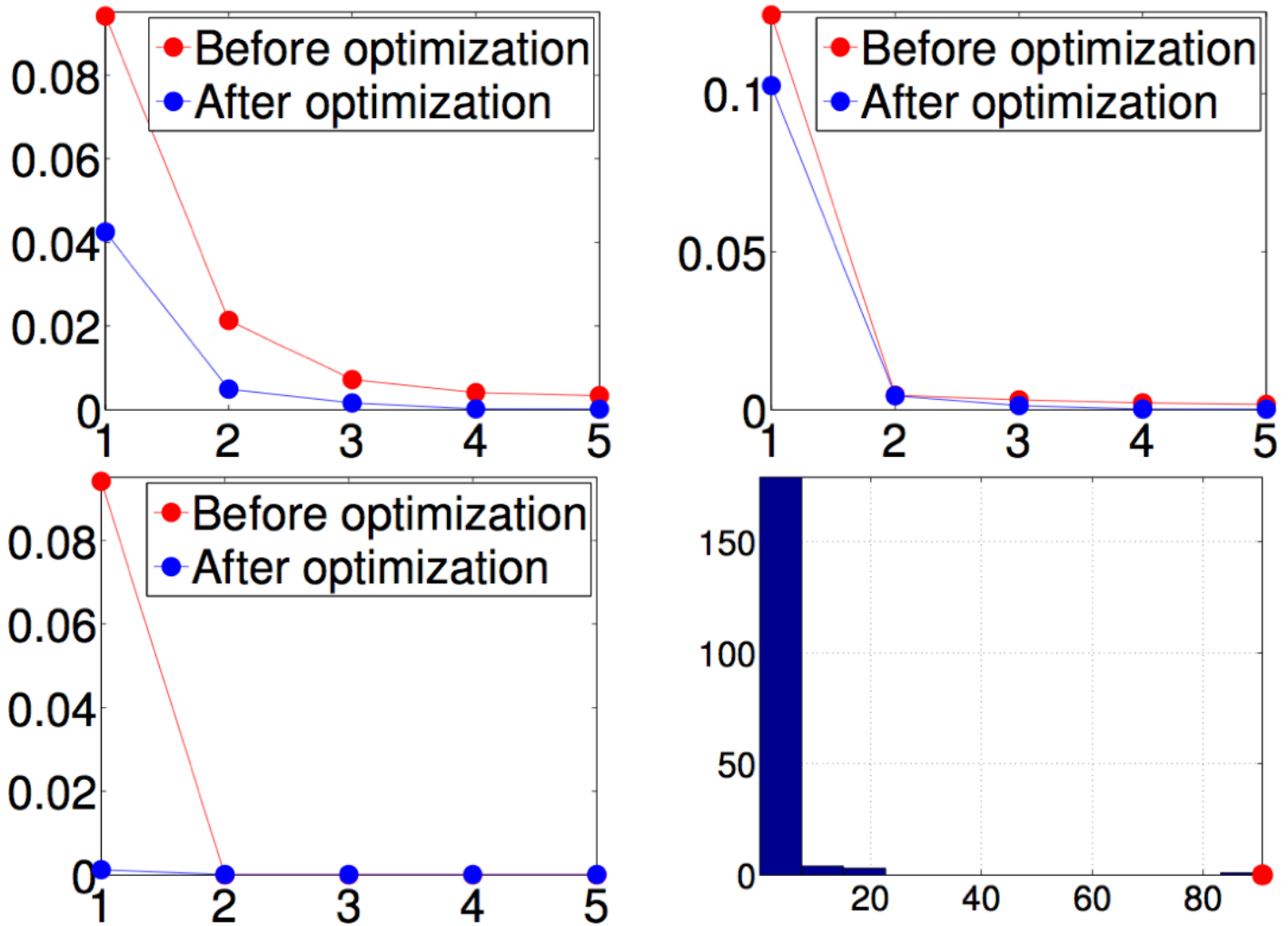


Figure 7: **Left Column, (Top-to-Bottom):** show the largest 5 eigen values of the covariance matrices C_1 and C_2 , respectively, before and after EM optimization. **Right Column, Top:** show the largest 5 eigen values of the covariance matrices C , before and after EM optimization. **Right Column, Bottom:** shows the histogram of Hotelling's T^2 statistics obtained by permutation testing (200 randomly-chosen group-label permutations) and the T^2 statistic for the non-permuted groups (red dot).

6.2 Results on a Database of Leaves

Figure 6 shows the 2 leaf groups that presents a challenge for hypothesis testing because the differences between the leaves are subtle. Figure 7 shows the results of permutation testing indicating the the non-permuted labeling produces the most extreme statistic (p value = 0.005) thereby leaning significantly towards rejection of the null hypothesis underlying permutation testing. This is the desired result because the two leaf groups were known to correspond to two different tree species.

7 Application II — Classification

After the multi-group model is fit to *training* data, we can classify unseen shapes as follows. The *test* pointset is first Procrustes aligned to the population mean yielding a pointset, say, z . Let the hidden random variable corresponding to the test shape be w . Then, we evaluate the probability of the unseen shape z being drawn from the each group model, i.e., $P(z|M_1, C_1, \beta_1)$ and $P(z|M_2, C_2, \beta_2)$

and classify z to the class that yields a higher probability. We can evaluate the aforementioned probabilities as follows:

$$\begin{aligned}
P(z|M_1, C_1, \beta_1) &= \int_w P(z, w|M_1, C_1, \beta_1)dw \\
&= \int_w P(z|w, M_1, C_1, \beta_1)P(w|M_1, C_1, \beta_1)dw \\
&\approx \sum_{s=1}^S \frac{1}{S} P(z|w^s) \text{ where } w^s \sim P(W|M_1, C_1, \beta_1).
\end{aligned} \tag{12}$$

7.1 Results on a Database of Leaves

We performed the classification task by training using only 3 leaves from each group and testing on the remaining 20 leaves in each group. We obtained a correct-classification rate of 97.5%.

8 Discussion and Conclusion

This paper propose a novel hierarchical graphical generative statistical model for modeling shapes (a shape is defined as an equivalence class of pointsets[12]) within a population for modeling multiple groups within a population. Model inference proceeds using the EM framework where the individual shape variables as well as the group-mean shape variables are treated as hidden random variables. In the E step, the approximation of the Q function using Monte-Carlo simulation entails sampling in Kendall shape space for which we propose a novel method that incorporates the (i) efficient HMC sampling coupled with (ii) gradient projection on shape manifolds. We validate the proposed modeling and inference scheme on simulated box-bump shapes[13] and exploit the framework in two different applications, namely hypothesis testing and classification, where we obtain very promising results on a difficult real database. The framework could be extended for unsupervised learning of classes of shapes.

The proposed hierarchical graphical model is *not* a simple Gaussian graphical model because of (i) smoothness penalty on individual shape variables as well as (ii) the (nonlinear) current norm used to model the joint distribution of the observed pointset and the associated hidden shape variable. In this way, the proposed framework solves a non-trivial inference problem.

This paper does *not* model dependencies of the per-group covariances C_1, C_2 on appropriate population-level parameters. It also ignores smoothness parameters on the group means because of the limited practical use of these parameters given many observed datasets per group. These limitations can lead to areas for future work. Nevertheless, we believe that the paper still makes important contributions.

References

- [1] F Bookstein. *The measurement of biological shape and shape change*. Number 24 in Lect. Notes Biomath. Springer-Verlag, 1978.
- [2] J Cates, P. T. Fletcher, M Styner, H Hazlett, and R Whitaker. Particle-based shape analysis of multi-object complexes. In *Proc. Info. Process. Med. Imag.*, pages 477–485, 2008.
- [3] T Cootes, C Taylor, D Cooper, and J Graham. Active shape models - their training and application. *Computer Vision and Image Understanding*, 61(1):38–59, 1995.
- [4] J Coughlan and S Ferreira. Finding deformable shapes using loopy belief propagation. In *Proc. European Conference on Computer Vision*, pages 453–468, 2002.
- [5] R Davies, C Twining, T Cootes, and C Taylor. A minimum description length approach to statistical shape analysis. *IEEE Transactions on Medical Imaging*, 21(5):525–537, 2002.
- [6] A. P. Dempster, N. M. Laird, and D. B. Rubin. Maximum likelihood from incomplete data via the EM algorithm. *Journal of the Royal Statistical Society*, B(39):1–38, 1977.
- [7] I Dryden and K Mardia. *Statistical Shape Analysis*. John Wiley and Sons, 1998.
- [8] S Duane, A Kennedy, B Pendleton, and D Roweth. Hybrid Monte Carlo. *Physics Letters*, 195:216–222, 1987.
- [9] C Goodall. Procrustes methods in statistical analysis of shape. *Journal of the Royal Statistical Society*, 53(2):285–339, 1991.
- [10] L Gu and T Kanade. A generative shape regularization model for robust face alignment. In *Proc. Euro. Conf. Computer Vision*, pages 413–426, 2008.

- [11] S Joshi, R Kommaraji, J Phillips, and S Venkatasubramanian. Comparing distributions and shapes using the kernel distance. In *Proc. 27th annual ACM symposium on Computational geometry*, pages 47–56, 2011.
- [12] D Kendall. Shape manifolds, Procrustean metrics, and complex projective spaces. *Bull. London Math. Soc.*, 16(2):81–121, 1984.
- [13] A Kotcheff and C Taylor. Automatic construction of eigen shape models by direct optimization. *Medical Image Analysis*, 2(4):303–314, 1998.
- [14] LEAF. Tree Leaf Database, Inst. of Information Theory and Automation ASCR, Prague, Czech Republic, http://zoi.utia.cas.cz/tree_leaves, 2012.
- [15] R Neal. An improved acceptance procedure for hybrid Monte Carlo algorithm. *J. Comput. Physics*, 111:194–203, 1994.
- [16] R Neal. *Bayesian learning for neural networks*. Springer-Verlag, 1996.
- [17] R Neal. MCMC using Hamiltonian dynamics. *Handbook of Markov Chain Monte Carlo*, Chapman and Hall, CRC Press, pages 113–162, 2010.
- [18] A Neumann. Graphical Gaussian shape models and their application to image segmentation. *IEEE Trans. Pattern Analysis and Machine Intelligence*, 25(3):316–329, 2003.
- [19] I Oguz, M Niethammer, J Cates, R Whitaker, P. T. Fletcher, C Vachet, and M Styner. Cortical correspondence with probabilistic fiber connectivity. In *Proc. Info. Processing Med. Imaging*, pages 651–663, 2009.
- [20] A Rangarajan, J Coughlan, and A Yuille. A Bayesian network framework for relational shape matching. In *Proc. Int. Conf. Computer Vision*, pages 671–678, 2003.
- [21] H Thodberg. MDL shape and appearance models. In *Proc. Info. Processing Med. Imaging*, volume 2, pages 251–260, 2003.
- [22] M Vaillant and J Glaunes. Surface matching via currents. In *Proc. Info. Processing Med. Imaging*, volume 19, pages 381–92, 2005.
- [23] Song-Chun Zhu. Embedding Gestalt laws in Markov random fields. *IEEE Trans. Pattern Analysis and Machine Intelligence*, 21(11):1170–1187, 1999.